

Domain-Aware SE Network for Sketch-based Image Retrieval with Multiplicative Euclidean Margin Softmax

Peng Lu
Shenzhen International Graduate
School, Tsinghua University
Shenzhen, China
lup21@mails.tsinghua.edu.cn

Gao Huang
Department of Automation, Tsinghua
University
Beijing, China
gaohuang@tsinghua.edu.cn

Hangyu Lin
School of Data Science, Fudan
University
Shanghai, China
linhy960303@gmail.com

Wenming Yang*
Shenzhen International Graduate
School & Department of Electronic
Engineering, Tsinghua University
Shenzhen, China
yang.wenming@sz.tsinghua.edu.cn

Guodong Guo
IDL, Baidu Research
National Engineering Lab for Deep
Learning Technology and Application
Beijing, China
guoguo01@baidu.com

Yanwei Fu†
School of Data Science, Fudan
University
Shanghai, China
yanweifu@fudan.edu.cn

ABSTRACT

This paper proposes a novel approach for Sketch-Based Image Retrieval (SBIR), for which the key is to bridge the gap between sketches and photos in terms of the data representation. Inspired by channel-wise attention explored in recent years, we present a Domain-Aware Squeeze-and-Excitation (DASE) network, which seamlessly incorporates the prior knowledge of sample sketch or photo into SE module and make the SE module capable of emphasizing appropriate channels according to domain signal. Accordingly, the proposed network can switch its mode to achieve a better domain feature with lower intra-class discrepancy. Moreover, while previous works simply focus on minimizing intra-class distance and maximizing inter-class distance, we introduce a loss function, named Multiplicative Euclidean Margin Softmax (MEMS), which introduce multiplicative Euclidean margin into feature space and ensure that *the maximum intra-class distance is smaller than the minimum inter-class distance*. This facilitates learning a highly discriminative feature space and ensures a more accurate image retrieval result. Extensive experiments are conducted on two widely used SBIR benchmark datasets. Our approach achieves better results on both datasets, surpassing the state-of-the-art methods by a large margin.

CCS CONCEPTS

• **Computing methodologies** → **Visual content-based indexing and retrieval.**

*indicates corresponding author.

†Yanwei Fu is with the School of Data Science, MOE Frontiers Center for Brain Science, and Shanghai Key Lab of Intelligent Information Processing, Fudan University.

Permission to make digital or hard copies of all or part of this work for personal or classroom use is granted without fee provided that copies are not made or distributed for profit or commercial advantage and that copies bear this notice and the full citation on the first page. Copyrights for components of this work owned by others than ACM must be honored. Abstracting with credit is permitted. To copy otherwise, or republish, to post on servers or to redistribute to lists, requires prior specific permission and/or a fee. Request permissions from permissions@acm.org.

MM '21, October 20–24, 2021, Virtual Event, China

© 2021 Association for Computing Machinery.

ACM ISBN 978-1-4503-8651-7/21/10...\$15.00

<https://doi.org/10.1145/3474085.3475499>

KEYWORDS

Sketch-based Image Retrieval, Multiplicative Euclidean Margin, Domain-Aware SE, Hashing

ACM Reference Format:

Peng Lu, Gao Huang, Hangyu Lin, Wenming Yang, Guodong Guo, and Yanwei Fu. 2021. Domain-Aware SE Network for Sketch-based Image Retrieval with Multiplicative Euclidean Margin Softmax. In *Proceedings of the 29th ACM International Conference on Multimedia (MM '21)*, October 20–24, 2021, Virtual Event, China. ACM, New York, NY, USA, 12 pages. <https://doi.org/10.1145/3474085.3475499>

1 INTRODUCTION

Touch-screen devices, such as smartphones and iPad, enable users to draw free-hand sketches conveniently. These sketches are highly iconic, succinct, and abstract representations, and usually convey richer and more accurate information than texts in various scenarios. Consequently, many novel applications related with sketch have sprung up. One representative example is the Sketch-Based Image Retrieval (SBIR), which has attracted great attention from the computer vision community during the past decades [15, 24, 24, 35, 37, 48, 53]. For the SBIR task, learning good representations for both sketches and photos is vital and remains a challenging problem [31, 32, 37, 40, 48, 49].

Given a query sketch, the objective of SBIR is to find relevant photos that are semantically related, e.g., they come from the same category (as shown in Figure 1). This task appears to be easy for humans but is difficult for a machine. The main challenge comes from the fact that there is a huge gap between the data representation in the two domains: the sketches are represented by highly iconic, abstract, and sparse lines, while the photos are composed of dense color pixels with rich texture information. This domain gap obstructs the SBIR model in exploiting the shared semantics and discriminative representations for both photos and sketches.

Recently, plenty of works have been proposed to address this problem. A popular approach is constructing an excellent intermediate representation, i.e., converting photos to edge maps [24, 37, 48, 53] or translating sketches into the photo domain using generative models [53]. Another widely adopted approach is learning

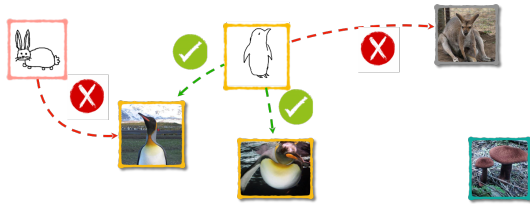


Figure 1: Illustration of SBIR task.

a semi-heterogeneous network in an end-to-end manner [24, 35]. These approaches have either large computation consumption or redundant parameters. On the contrary, TC-net [21] uses a single CNN to process both sketches and photos. High retrieval accuracy is achieved with this scheme. However, vanilla CNN is domain-agnostic and thus can not fully utilize the prior knowledge about which domain the sample comes from.

Therefore, we propose a Domain-Aware Squeeze-and-Excitation (DASE) network, which can embed sketches and photos respectively according to their domain with a negligible increase of computation and parameter. This function is achieved via DASE module. In vanilla SE module [11], the convolutional features are firstly squeezed into a low dimensional embedding by an encoder network, and then they are decoded to generate a channel-wise attention vector which is applied to the original feature maps. In DASE module, we simply append one binary-value code that indicates which domain the sample comes from, to the low dimensional embedding. With this modification, DASE module can emphasize different channels according to the domain knowledge. Extensive experiments prove that this change is simple yet highly effective.

Further, loss function is essential in learning a discriminative feature space. Specifically, to achieve high retrieval accuracy, an ideal feature criterion is expected where the maximum intra-class distance is less than the minimum inter-class distance. However, previous works on SBIR do not optimize networks toward this end. Cross-view Pairwise Loss [24] and Semantic Loss [53] are utilized to minimize intra-class distance and maximize inter-class distance in binary space. But they do not introduce any margin and guarantee the above ideal feature criterion. Moreover, these losses are difficult to optimize since they are non-convex and non-smooth, and optimization algorithms based on alternating iteration is required, which are very cumbersome.

In this work, we propose maximizing the inter-class distance to be several times the intra-class distance in Euclidean space. This enables us to derive a novel loss function – Multiplicative Euclidean Margin Softmax (MEMS), which controls the ratio of the intra-class and the inter-class distance jointly. With appropriate ratio, the maximum intra-class distance is less than the minimum inter-class distance. This loss can be easily optimized using back-propagation and can generate a discriminative feature space. Further, we provide theoretical analysis to explain how the MEMS loss works and give a lower bound of the multiplicative margin. Experiments show that the MEMS loss can yield highly accurate retrieval results, which surpass all existing algorithms by a large margin. The results generated by MEMS loss can be kept in a hashing scheme that converts learned features into low dimensional binary codes. This

post-processing step can be realized with a spectral normalized perception which is also easy to optimize. The experimental results validate the effectiveness of our model.

Contributions. The main contributions of this paper include: (1) A novel network architecture DASE is introduced to incorporate the additional information about the domain attribution, which boosts the retrieval performance with both shallow and deep networks; (2) A novel loss function, the Multiplicative Euclidean Margin Softmax (MEMS), that optimizes a discriminative feature space where the maximum intra-class distance is smaller than the minimum inter-class distance; (3) Theoretical analysis is provided on the properties of the MEMS loss; (4) New state-of-the-art results have been obtained on several competitive SBIR tasks.

2 RELATED WORK

SBIR. Sketch-Based Image Retrieval (SBIR) aims to retrieve similar semantic meaning images as the query sketch. A typical solution is to learn a shared embedding space for both sketches and images. Such a common space facilitates the ranking of similarity of sketches and images. Previous methods transfer photos into sketch-tokens and then extract hand-craft sketch features [5, 12, 27, 31] or deep features [24, 37, 40, 48, 49] to represent the sketches. Recent deep learning based architectures [18, 21, 29, 53] enable cross-domain learning in an end-to-end manner. To accelerate the retrieval in a large-scale dataset, hashing based models [24, 35, 47, 53] have also been studied.

Attention in CNNs. Attention mechanism enables networks to assign different significance on different parts of the input. The important feature expressions are amplified while the less useful ones are suppressed. To better apprehend digital images, many convolutional networks with spatial attention [4, 13, 19, 44] and channel-wise attention [2, 11] are proposed to emphasize the informative region or channels. SENet [11] proposes a squeeze-and-excitation structure. Global context is aggregated by global average pooling for each channel. The aggregated information is then processed and used to reallocate attention over channels by feature fusion. To tackle the SBIR problem, spatial attention [37, 50, 53] has been utilized. However, channel-wise attention has never been explored in cross-modal embedding for sketches and photos so far.

Loss functions. Many metric learning based methods [10, 28, 42, 45] proposed learning deep features by the loss functions with Euclidean distances. To make the learned features more discriminative, other variants of loss functions have been investigated recently, such as the contrastive loss [3, 9], triplet loss [34], and softmax-based losses [6, 25, 26, 41]. Particularly, the contrastive and triplet losses aim at increasing the Euclidean margin in an additive manner, which might be neglected as there is no upper bound for Euclidean distance. A-softmax [25] optimize the inter-class angular distance to be several times the intra-class angular distance to guarantee that the least inter-class distance is more than the largest intra-class distance. Furthermore, prototypical loss [36] is also a variant of softmax which incorporates the Euclidean distance.

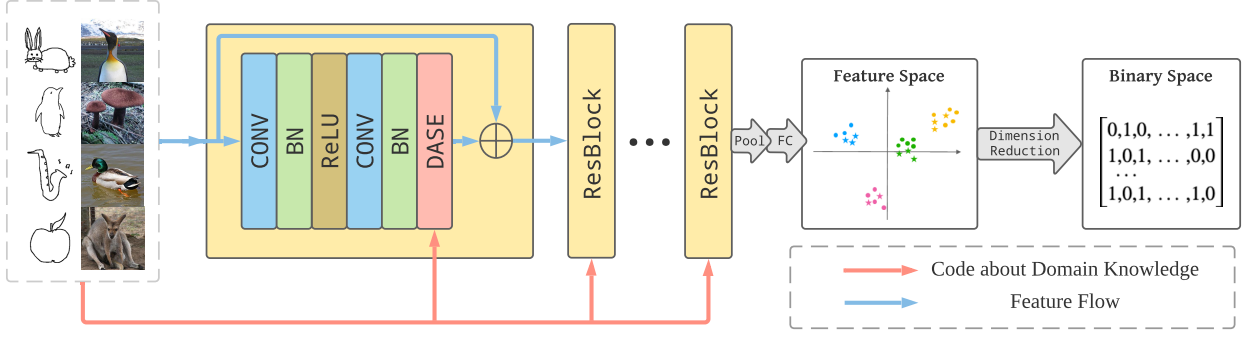


Figure 2: Illustration of our framework. We mix sketches and photos as input of the DASE network, to which the proposed DASE module is added. Domain knowledge is encoded in DASE modules in each ResBlock. After training, the output features or binarized code can be used to conduct SBIR, where Euclidean distance and Hamming distance are used as metric, respectively.

3 METHOD

In this section, we present the proposed DASE network and the MEMS loss for SBIR task in detail. The SBIR task is formulated as [24, 53]. We have the realistic photo set $\mathcal{P} = \{(p_i, y_i) \mid y_i \in \mathcal{Y}\}$, and the sketch set $\mathcal{S} = \{(s_j, y_j) \mid y_j \in \mathcal{Y}\}$ respectively. Given a query sketch, the objective of SBIR is to find all of its relevant photos that semantically belong to the same category as the sketch. As the setting defined in [24], the same photo set \mathcal{P} is used for both training and test, as the retrieval galleries. Sketch set \mathcal{S} is split into train and test sets, with the same label set \mathcal{Y} .

The feature representation networks of sketches and photos are denoted as \mathcal{F}_p and \mathcal{F}_s respectively. The two networks project sketches and photo to a shared space, i.e. $\mathcal{F}_p(p_i), \mathcal{F}_s(s_j) \in \mathcal{X}$; thus we have the set $\mathcal{D} = \{(x, y_x) \mid y_x \in \mathcal{Y}\}$, where the feature $x \in \mathcal{X}$ can come either from photo domain or sketch domain and the label y_x is identical with the source sample of feature x . We further introduce the denotation, $\mathcal{D}_y = \{x \mid y_x = y\}$ for convenience.

3.1 Overview

To facilitate learning feature representations for sketches and photos, the proposed Domain-Aware SE (DASE) network is shared by both domains. This network is composed of several ResBlocks in which the DASE module is inserted (see in Figure 2). In contrast to vanilla SE module [11], DASE module receives code about the domain of input image and emphasizes different channels individually. Further, to bridge the data representation gap between the sketch and photo domains, we present a novel loss function – Multiplicative Euclidean Margin Softmax (MEMS) loss, which can efficiently learn a unified embedding space. The MEMS loss optimizes the larger inter-class and smaller intra-class distance over the photo and sketch set. In other words, the instances of sketches and photos in the same/different class should be close/far from each other.

3.2 Domain-Aware SE Network

Learning common feature representations for sketch and photo domains is a non-trivial task. Obviously, sketches are iconic and abstract with various deformation levels; while photos are realistic images with rich color, texture, and shape information.

Rather than using independent sub-networks to process the photos and sketches separately, our model learns a single network

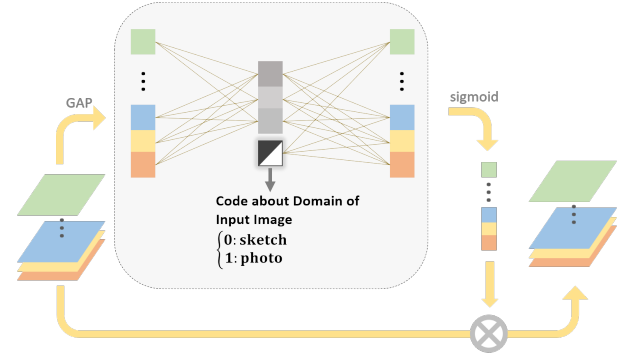


Figure 3: The structure of DASE module. The activation function for the intermediate FC layer is Sigmoid.

to analyze the photos and sketches jointly. Such a SiameseNet-like network is inspired by the fact that SiameseNet is efficient in learning the embedding space across different domains (e.g., image-text embedding [43], or person re-identification [38]). The semi-heterogeneous network is proposed in [24], including a shared Siamese sub-network and separate sub-networks for each domain.

In contrast to [24], we further propose Domain-Aware Squeeze-and-Excitation (DASE) module, which is shown in Figure 3, to learn an effective feature representation. Particularly, our DASE module is an extension of SE module [11] which provides an explicit mechanism to re-weight the importance of channels after each block in the network. As shown in Figure 3, our DASE module utilizes an encoder-decoder structure followed by a sigmoid activation. Within the intermediate space, a *binary code* is added to indicate whether the input image is a sketch or a photo. The outputs of sigmoid activation are the feature attention vector over channels. This conditional structure can thus help capture different characteristics of input images conditioned on which domain they come from.

With the DASE module, our feature extractor, which is a Siamese Network with the domain-conditioned structure, is learned over two domains to explore shared semantics in a common feature space. The binary code serves as a controlling gate and endows the flexibility of network in learning from each individual domain.

3.3 Multiplicative Euclidean Margin Softmax Loss

The loss function is vital in successfully optimizing the networks over the recognition tasks, especially in our cross-domain scenario. To embed the photo and sketch into a shared space, we propose the Multiplicative Euclidean Margin Softmax loss, which exploits the strategy of maximizing the intra-class distance and minimizing the inter-class distance.

Given the category $y \in \mathcal{Y}$, the maximum intra-class distance can be defined by $\max_{\mathbf{x}, \mathbf{x}' \in \mathcal{D}_y} d(\mathbf{x}, \mathbf{x}')$ and the minimum inter-class distance would be $\min_{\mathbf{x} \in \mathcal{D}_y, \mathbf{x}' \in (\bigcup_{y' \neq y} \mathcal{D}_{y'})} d(\mathbf{x}, \mathbf{x}')$, where $d(\cdot, \cdot)$ can be any kind of differentiable distance metric. Thus to develop our formulation, we optimize our framework by enforcing that the maximum intra-class distance to be smaller than minimum inter-class distance,

$$\forall y \in \mathcal{Y}, \max_{\mathbf{x}, \mathbf{x}' \in \mathcal{D}_y} d(\mathbf{x}, \mathbf{x}') \leq \min_{\mathbf{x} \in \mathcal{D}_y, \mathbf{x}' \in (\bigcup_{y' \neq y} \mathcal{D}_{y'})} d(\mathbf{x}, \mathbf{x}'). \quad (1)$$

Rather than directly optimizing Eq (1) over all instances, we compute the prototypes $\{\mathbf{c}_y\}_{y \in \mathcal{Y}} \subset \mathcal{X}$ of each class, and characterize the distribution of instances in feature space. If MEMS loss is well optimized, instances will be closer to their corresponding prototype than other prototypes in feature space. This is as,

$$\forall (\mathbf{x}, y_x) \in \mathcal{D}, \forall y \in \mathcal{Y} \wedge y \neq y_x, m \cdot d(\mathbf{x}, \mathbf{c}_{y_x}) \leq d(\mathbf{x}, \mathbf{c}_y), \quad (2)$$

where $m \geq 1$ is referred to as the margin constant.

For convenience, we denote $\mathcal{R}_{y,y'}$ as a region in the feature space,

$$\mathbf{x} \in \mathcal{R}_{y,y'} \Leftrightarrow m \cdot d(\mathbf{x}, \mathbf{c}_y) \leq d(\mathbf{x}, \mathbf{c}_{y'}).$$

Also, we denote \mathcal{R}_y as a region such that

$$\mathbf{x} \in \mathcal{R}_y \Leftrightarrow \forall y' \in \mathcal{Y} \wedge y' \neq y, m \cdot d(\mathbf{x}, \mathbf{c}_y) \leq d(\mathbf{x}, \mathbf{c}_{y'}),$$

which takes account different data distributions of each class. It is easy to prove that $\mathcal{R}_y = \bigcap_{y' \neq y} \mathcal{R}_{y,y'}$. Note that if Eq (2) holds,

$$\forall (\mathbf{x}, y_x) \in \mathcal{D}, \mathbf{x} \in \mathcal{R}_{y_x},$$

and thus we can derive a sufficient condition for Eq. (1),

$$\forall y \in \mathcal{Y}, \max_{\mathbf{x}, \mathbf{x}' \in \mathcal{R}_y} d(\mathbf{x}, \mathbf{x}') \leq \min_{\mathbf{x} \in \mathcal{R}_y, \mathbf{x}' \in (\bigcup_{y' \neq y} \mathcal{R}_{y'})} d(\mathbf{x}, \mathbf{x}'). \quad (3)$$

MEMS loss. To incorporate this understanding and optimize Eq (2) by softmax loss, this gives us a novel loss function– Multiplicative Euclidean Margin Softmax (MEMS) loss:

$$\mathcal{L}_{ems} = \frac{1}{N} \sum_{i=1}^N -\log \frac{e^{-m^2 \|\mathbf{x}_i - \mathbf{c}_{y_i}\|_2^2}}{e^{-m^2 \|\mathbf{x}_i - \mathbf{c}_{y_i}\|_2^2} + \sum_{j \neq y_i} e^{-\|\mathbf{x}_i - \mathbf{c}_j\|_2^2}}, \quad (4)$$

where \mathbf{x}_i indicates the feature extracted by the last layer of feature representation network. \mathbf{c}_j is the center of j -th category. We take the center \mathbf{c}_j as the parameters, and update \mathbf{c}_j dynamically, rather than directly using the average feature center. In Eq (4), we employ the negative squared Euclidean distance to measure the confidence of \mathbf{x}_i being $(-\|\mathbf{x}_i - \mathbf{c}_j\|_2^2)$. Particularly, in binary classification, \mathbf{x}_i is labelled as class 1 if $m \|\mathbf{x} - \mathbf{c}_1\|_2 < \|\mathbf{x} - \mathbf{c}_2\|_2$, and otherwise, as class 2.

3.4 Theoretical analysis and lower bound of m

The property of MEMS is largely determined by the value of m . Intuitively, a larger m makes decision boundaries closer to corresponding prototypes and the distribution of features more compact. This produces a more discriminative metric space. However, overly large m tends to make the training process unstable due to the inherent variances among samples in each category.

Therefore, it is necessary to find the minimum m to ensure that, for every sample, and in metric space, the maximum intra-class distance is smaller than minimum inter-class distance. We give some theoretical analysis about the Eq (2) and Eq (3). Most importantly, if we adopt Euclidean distance as $d(\cdot, \cdot)$, $m \geq 2 + \sqrt{3}$ is the sufficient and necessary condition for Eq (3) given Eq (2). We show a brief proof below and the details can be found in Appendix.

Sufficient. If $d(\mathbf{x}, \mathbf{x}') = \|\mathbf{x} - \mathbf{x}'\|_2$, $\mathcal{R}_{y,y'}$ is a n -ball (ball in n -dimensional space) with the center $(\mathbf{c}_y + (\mathbf{c}_y - \mathbf{c}_{y'}) / (m^2 - 1))$ and the radius $(m/m^2 - 1) \|\mathbf{c}_y - \mathbf{c}_{y'}\|_2$. Thus in binary categorization, the minimum value of m is $2 + \sqrt{3}$. With the growth of the number of categories, the minimum value is reduced monotonously. So it is sufficient to have $m \geq 2 + \sqrt{3}$ guaranteeing perfect discrimination. **Necessary.** We illustrate the necessity in multi-class cases, since, if two prototypes are far from the others, their relationship will resemble the one in binary case. So $m \geq 2 + \sqrt{3}$ is necessary regardless of the number of categories.

3.5 Differences with other losses

We further discuss the differences between our MEMS loss and other losses.

Prototypical loss [36] It is defined as

$$\mathcal{L}_{proto} = \frac{1}{N} \sum_i^N -\log \frac{e^{-\|\mathbf{x}_i - \mathbf{c}_{y_i}\|_2^2}}{\sum_j e^{-\|\mathbf{x}_i - \mathbf{c}_j\|_2^2}}. \quad (5)$$

The prototypical loss is used in one-shot classification where only a few training instances are available for each class. Thus \mathbf{c}_j is directly computed as the averaged mean of training instances; in contrast, our MEMS loss is a generalized softmax loss, and optimizes \mathbf{c}_j via back-propagation. Furthermore, the prototypical loss is a special case of MEMS loss when the margin is 1. It is sufficient for classification task and insufficient for training a discriminative feature space for retrieval task. Therefore a margin constant m is introduced to make a balance between enlarging the inter-class distance and shrinking the intra-class distance.

Angular Margin loss. We further discuss the difference between MEMS loss and angular margin loss. Similar to Euclidean distance, angular distance based loss functions, such as A-Softmax [25] and LMCL [41], are also employed in learning a shared space in many tasks, e.g., face recognition. These angular margin losses aim at learning a discriminative distribution on a hypersphere. As shown in Table 1, they define different similarity functions for the instances of different classes. Note that $\psi(\theta)$ is an artificial piece-wise function that serves as the extension of $\cos(m \cdot \theta)$, to overcome its non-monotonicity. Nevertheless, it is non-trivial to define the $\psi(\theta)$ in A-softmax function as stated in [41]. The scalar s in LMCL is used to expand the range of similarity function; otherwise, the output of softmax function would be closed to the uniform distribution over all categories.

Similarity	intra-class	inter-class ($j \neq y_i$)
A-Softmax	$\ \mathbf{x}_i\ _2 \cdot \psi(\theta_{y_i})$	$\ \mathbf{x}_i\ _2 \cdot \cos(\theta_j)$
LMCL	$s \cdot (\cos(\theta_{y_i}) - m)$	$s \cdot \cos(\theta_j)$
MEMS (ours)	$-m^2 \ \mathbf{x}_i - \mathbf{c}_{y_i}\ _2^2$	$-\ \mathbf{x}_i - \mathbf{c}_j\ _2^2$

Table 1: The similarity functions of A-Softmax, LMCL and MEMS loss. θ_y represents angular distance between the feature vector and the prototype of category y .

Triplet loss [34] It is defined as

$$\mathcal{L}_{tri} = \sum_i \left[\left\| \mathbf{x}_i^a - \mathbf{x}_i^p \right\|_2^2 - \left\| \mathbf{x}_i^a - \mathbf{x}_i^n \right\|_2^2 + \alpha \right]_+, \quad (6)$$

where \mathbf{x}_i^a and \mathbf{x}_i^p share same class while \mathbf{x}_i^a and \mathbf{x}_i^n come from different class. α is the margin between the distance of positive pairs and negative pairs. Different from the proposed MEMS loss, this margin is additive and can not ensure that the *maximum* intra-class distance is smaller than the *minimum* inter-class distance. In addition, triplet loss computes the distance between two instance pairs, and its sampling complexity is $\mathcal{O}(N^3)$. By contrast, the sampling complexity of MEMS loss is $\mathcal{O}(N)$ as it computes distance between each instance and prototypes.

4 EXPERIMENTS

4.1 Datasets and Settings

Datasets. Our model is evaluated on two large-scale sketch-photo datasets: TU-Berlin [8] Extension and Sketchy [33] Extension. The former includes 20,000 sketches uniformly distributed among 250 categories. Additionally, 204,489 natural images provided in [52] are utilized as the photo gallery. The Sketchy database consists of 75,471 hand-drawn sketches and 12,500 corresponding photos from 125 categories. It was extended by another 60,502 photos for SBIR task in [24]. Following the settings in [24, 53], 10/50 sketches from each category are picked as the query set for TU-Berlin/Sketchy dataset, and the rest are used for training. All gallery photos are used in both training and testing phases.

Implementation. Our method is implemented using Pytorch with single 1080Ti GPU. We use Adam optimizer [16] with parameters $\beta_1 = 0.9$, $\beta_2 = 0.999$, $\lambda = 0.0001$. The learning rate is set to 0.0001 and linearly decays to 0 during the second half of training. The model converges after training for 200k iterations. We use the backbone network of ResNeXt-101, which is composed of 33 ResNeXt Blocks. The proposed DASE module is added in each block. We use $m = 4$ in the proposed MEMS loss. Our code is available at: <https://github.com/Ben-Louis/SBIR-DASE-MEMS>

SBIR hashing. SBIR can be conducted using either real-value or binary-value vectors as features. The latter is named *SBIR hashing*, which greatly accelerates the speed of SBIR tasks but requires auxiliary design or process. The proposed method can generate both styles of features. Particularly, for SBIR hashing, we utilize a simple hashing scheme to encode the features \mathbf{x}_i generated by our network from one sketch s_i or a photo p_i . Our hashing scheme uses a spectral normalized perception \mathcal{F}_{SN} and a sign function to

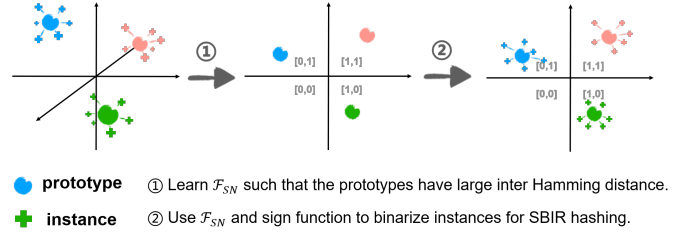


Figure 4: Visualization of hashing process.

Methods	TU-Berlin Extension	Sketchy Extension
HOG [5]	0.091	0.115
GF-HOG [12]	0.119	0.157
SHELO [31]	0.123	0.182
LKS [32]	0.157	0.190
CCA [39]	0.366	0.705
XQDA [20]	0.201	0.557
PLSR [23]	0.141	0.462
CVFL [46]	0.289	0.675
Siamese CNN [30]	0.322	0.481
SaN [49]	0.154	0.208
GN Triplet [33]	0.187	0.529
3D Shape [40]	0.072	0.084
Siamese-AlexNet [24]	0.367	0.518
Triplet-AlexNet [24]	0.448	0.573
DASE+Prototypical loss [36]	0.433	0.851
DASE+Triplet [34]	0.523	0.882
DASE+Softmax	0.772	0.929
DASE+A-Softmax [25]	0.815	0.938
DASE+LMCL [41]	0.837	0.950
ResNeXt+MEMS	0.798	0.949
DASE+MEMS (ours)	0.841	0.958

Table 2: MAP results of SBIR on TU-Berlin Extension and Sketchy Extension datasets.

projects \mathbf{x}_i into a low-dimensional binary space. This is a post-processing step after training CNNs. Specifically, the \mathcal{F}_{SN} is optimized by

$$\mathcal{L}_{hash} = \frac{1}{K(K-1)} \sum_j \sum_{k \neq j} \frac{\mathcal{F}_{SN}(\mathbf{c}_j)}{|\mathcal{F}_{SN}(\mathbf{c}_j)|} \cdot \frac{\mathcal{F}_{SN}(\mathbf{c}_k)}{|\mathcal{F}_{SN}(\mathbf{c}_k)|}, \quad (7)$$

where K is the number of categories and $|\cdot|$ represents element-wise absolute value. Note that $\mathcal{F}_{SN}(\mathbf{x}) = \mathbf{W}_{SN} \cdot \mathbf{x} + \mathbf{b}$, where \mathbf{W}_{SN} is a spectral normalized matrix and \mathbf{b} represents bias. This loss forces the prototype \mathbf{c}_j to have a large Hamming distance to each other in the low-dimension space. As \mathcal{F}_{SN} is spectral normalized, the Lipschitz constant of the mapping function from feature space to low-dimensional space (before binarization) is 1. Thus the property of Euclidean distance among instances, large inter-class distance and small intra-class distance, is kept in target low-dimensional space. After sign function, instances in the same class will have closed binary representation. The visualization of this process is shown in Figure 4.

Methods	TU-Berlin Extension			Sketchy Extension		
	32 bits	64 bits	128 bits	32 bits	64 bits	128 bits
CMFH [7]	0.149	0.202	0.180	0.320	0.490	0.190
CMSSH [1]	0.121	0.183	0.175	0.206	0.211	0.211
SCM-Seq [51]	0.211	0.276	0.332	0.306	0.417	0.671
SCN-Orth [51]	0.217	0.301	0.263	0.346	0.536	0.616
CVH [17]	0.214	0.294	0.318	0.325	0.525	0.624
SePH [22]	0.198	0.270	0.282	0.534	0.607	0.640
DCMH [14]	0.274	0.382	0.425	0.560	0.622	0.656
DSH [24]	0.358	0.521	0.570	0.653	0.711	0.783
GDH [53]	0.563	0.690	0.651	0.724	0.811	0.784
DASE+Prototypical loss [36]	0.381	0.395	0.400	0.833	0.845	0.850
DASE+Triplet [34]	0.510	0.519	0.527	0.874	0.882	0.885
DASE+Softmax	0.734	0.750	0.755	0.919	0.922	0.923
DASE+A-Softmax [25]	0.783	0.800	0.800	0.925	0.928	0.927
DASE+LMCL [41]	0.762	0.805	0.818	0.932	0.935	0.935
DASE+MEMS (ours)	0.819	0.824	0.829	0.948	0.953	0.956

Table 3: MAP results of SBIR hashing. Our model is compared against the previous SBIR methods on TU-Berlin Extension and Sketchy Extension. 32, 64, and 128 represents the length of generated hashing codes.

4.2 Results on Supervised SBIR

Competitors. We compare several competitors in Table 2: (1) hand-craft feature based models: LSK [32], SEHLO [31], HOG [5] and GF-HOG [12]; (2) cross-view feature embedding methods: CCA [39], PLSR [23], XQDA [20] and CVFL [46]; (3) deep learning based models: 3D Shape [40], Sketch-a-Net (SaN) [49], GN Triplet [33], Siamese CNN [30], Siamese-AlexNet, Triplet-AlexNet [24]. (4) Prototypical loss [36], Triplet loss [34], Softmax, A-Softmax [25] and LMCL [41] implemented with the same backbone network as our method. We use hyperparameters of A-Softmax [25] and LMCL [41] proposed in their papers. The Mean Average Precision (MAP) is reported.

Results. The results are summarized in Table 2. Obviously, our model outperforms all the competitors by a very large margin. It achieves a MAP improvement of 0.393/0.385 over the state-of-the-art real-valued based method – Triplet-AlexNet. This demonstrates the efficacy of our model. Note that the improved performance is due to the novel structure, and the MEMS loss function used here. We give further analysis in the ablation study in Section 4.4.

The effect of each component in our framework can be found in Table 2. We can conclude that the proposed MEMS loss and DASE module both improve the performance on SBIR task significantly.

4.3 Results on Supervised SBIR Hashing

Competitors. (1) Our hashing model is compared against 8 cross-modal hashing methods: Collective Matrix Factorization Hashing (CMFH) [7], Cross-Modal Semi-Supervised Hashing (CMSSH) [1], Cross-View Hashing (CVH) [17], Semantic Correlation Maximization (SCMSeq and SCM-Orth) [51], Semantics-Preserving Hashing (SePH) [22], Deep CrossModality Hashing (DCMH) [14], Deep Sketch Hash (DSH) [24] and Generative Domain-Migration Hashing (GDH) [53]. (2) Other softmax based loss functions implemented with the same backbone as our method: Prototypical loss [36],

Backbone	Methods	TU-Berlin Extension	Sketchy Extension	FLOPS
AlexNet	DSH [24]	0.570	0.783	1.65G
	DASE+MEMS (ours)	0.586	0.875	1.13G
Resnet-18	GDH [53]	0.690	0.811	16.93G
	DASE+MEMS (ours)	0.736	0.940	1.83G

Table 4: MAP results achieved with same backbone network. DSH [24] modifies AlexNet to a semi-heterogeneous network; GAN is used in GDH [53] besides backbone network; we only append backbone network with DASE modules.

Triplet loss [34], Softmax, A-Softmax [25] and LMCL [41]. We use hyperparameters of A-Softmax [25] and LMCL [41] proposed in their papers. We still report the MAP.

Training cost. Our hashing scheme is taken as a post-processing step, in order to make our framework comparable to previous hashing based SBIR models. With our computed features, the hashing scheme is trained for 10000 steps; and the whole process can be finished in 1 minute on our computer.

Results. We summarize our results in Table 3. Our method achieves the best performance among all hashing-based methods and cross-modal learning methods. Critically, our model improves MAP with a scale over 0.13 in all conditions compared with GDH [53] which is the state-of-the-art method on this task. This further demonstrates the effectiveness of our framework in the SBIR hashing task. Some query examples with top-10 retrieval results are shown in Figure 5.

We also highlight that, although angular margin losses, particularly LMCL, can achieve comparable performance with MEMS in SBIR tasks, they suffer from a significant degradation in SBIR hashing. This degradation might be due to the property of angular distance, as it is more difficult to maintain in the dimension reduction mapping than Euclidean distance.

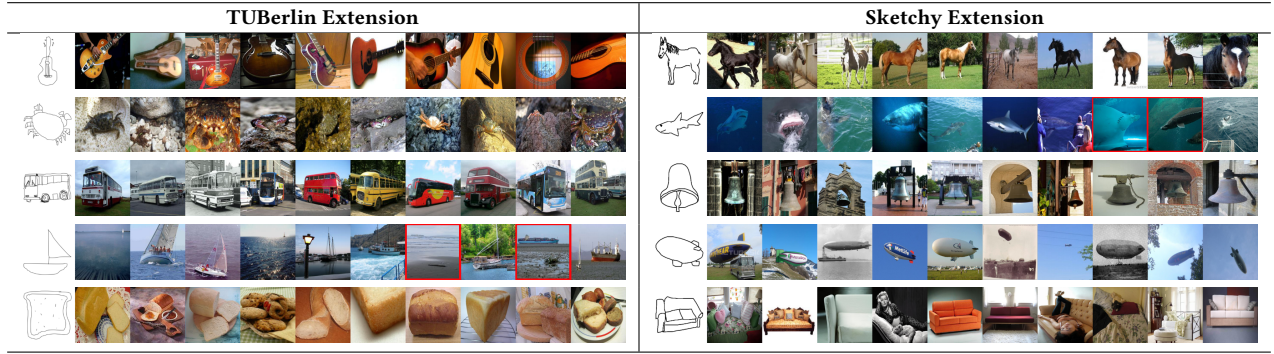


Figure 5: Visualization of retrieved images on both datasets. The red panes represent false retrieval results.

Comparison using same backbone. To emphasize the efficiency and efficacy of our model, we compare the MAP with state-of-the-art methods DSH [24] and GDH [53] using the same backbone networks, which is Alexnet and Resnet-18 respectively. The result is displayed in Table 4. The proposed method achieves higher MAP than other methods with much lower computation consumption.

Besides, our model can be trained efficiently. We only need to train a single network in an end-to-end manner without any domain translation process. On the contrary, GDH [53] utilized the cycle-consistent GANs to transfer sketches into photos. DSH [24] requires the pre-computed edge maps to bridge the gap between sketches and photos, and semantic representation (wordvec) is used as prior of inter-relationship among categories.

4.4 Ablation Study

To further investigate the propose approach, we conduct a series of ablation studies on both datasets.

Network modules. We compare two types of CNNs as well as their variants with SE modules [11] and the newly DASE modules. Intrinsically, the SE and DASE module can enhance the ability to learn different attention over feature channels, and thus enable a dynamic and implicit feature selection mechanism to our networks. The MAP results are shown in Figure 6. Both networks are trained and tested in the same setting; and *the same MEMS loss is used for all the networks*. We can find that SE module enhances the ability of CNNs to process inputs from multi-domains. Moreover, our DASE module is better than SE module on SBIR task, since the auxiliary binary code is introduced to make SE better learn to select important sketch/photo feature channels. DASE module can improve the performance of both deep and shallow networks. Particularly, on Resnet-18/ResNeXt-101, the auxiliary DASE modules have brought the MAP increase with 0.025/0.043 on TU-Berlin Extension and 0.011/0.009 on Sketchy Extension, respectively.

We also visualize the input feature maps of DASE modules in Figure 7. It is noticeable that some convolution kernels that can effectively extract content-related features from sketches might fail to extract such features from photos, and vice versa. Specifically, features in B2C239 generally respond to dark areas, and thus miss the key object in photos but capture crucial corners in sketches. On the contrary, in B6C17, sketch features show severe corner and edge effects which distort the semantic, while photo features respond to

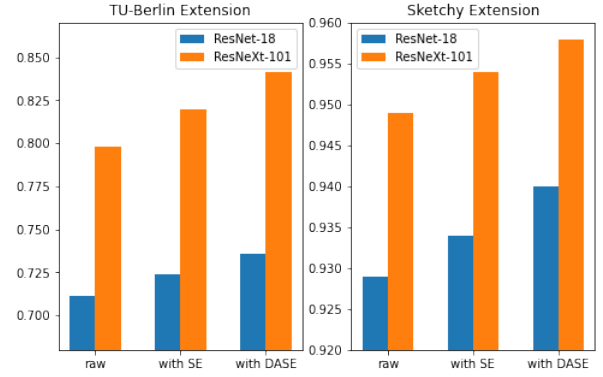


Figure 6: Performance of different network variants; all of which are pre-trained on ImageNet. We use MEMS loss with $m = 4$ to train these networks.

correct area. With prior knowledge, the DASE module can learn to amplify content-related features and suppress style-related features. The weight in the second fully-connected layer in DASE module associated with the binary code about input domain and B2C239 is -0.32, smaller than most channels, indicating that this channel is relatively amplified/suppressed when the input is a sketch/photo, respectively. As for B6C17, this weight is 0.30, and is larger than most channels, meaning that the photo features are amplified and the sketch features are suppressed.

The effects of different margin m . Performance of our model grows with the increase of value m , because it forces the network to learn discriminative representations. But when m is too large, e.g., $m > 4$, the performance stops rising and even begins falling, which is shown in Figure 8.

As revealed in Figure 9: (1) when $m = 1$, the intra-class distances of part of instances are greater than the minimum inter-class distance, which leads to bad retrieval performance; (2) when $m = 4$ and $m = 16$, the minimum inter-class distances are greater than intra-class distances generally, which explains the better performance in these cases. Nevertheless, the standard deviation within some categories does not decrease with larger m due to intrinsic variance, explaining why the performance stops rising or begins falling when m is overly large.

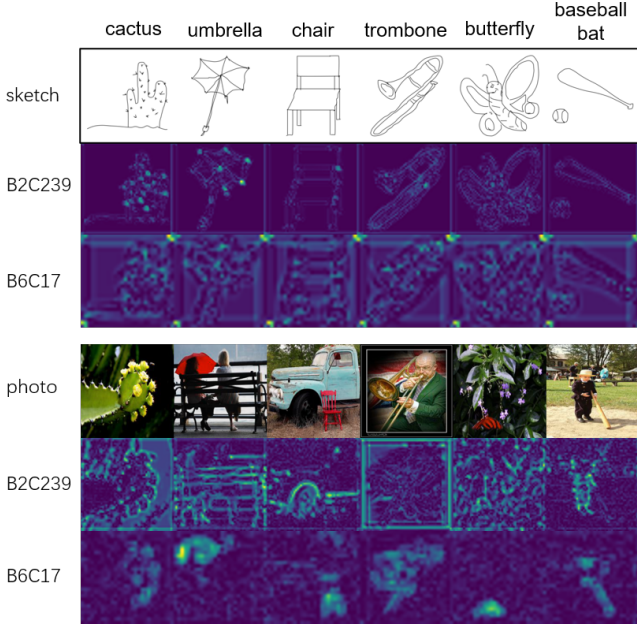


Figure 7: Visualization of feature maps amplified/suppressed by DASE. B2C239 refers to the 239-th channel of input feature map to the DASE module in second convolution block. B6C17 refers to the 17-th channel and 6-th convolution block.

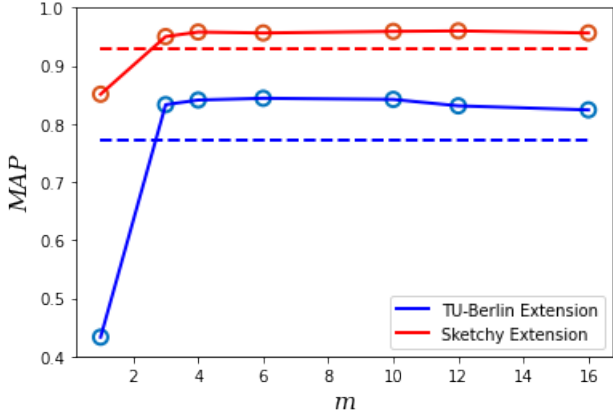


Figure 8: The MAP on two datasets with varying m in MEMS loss. The dashed lines represent the results of softmax on each dataset.

Analysis of the mapping in hashing. We train a spectral normalized fully-connected layer \mathcal{F}_{SN} for hashing. But the mapping can be modeled by other structures. We try fully-connected networks with different depth and settings (w./w.o. spectral normalization) for the hashing task. Note that if we adopt multi-layer networks, the dimension of intermediate layers is set to 256, and the activation function is Rectified Linear Unit, as the Lipschitz constant of ReLU is smaller than 1. The results of MAP on both datasets are

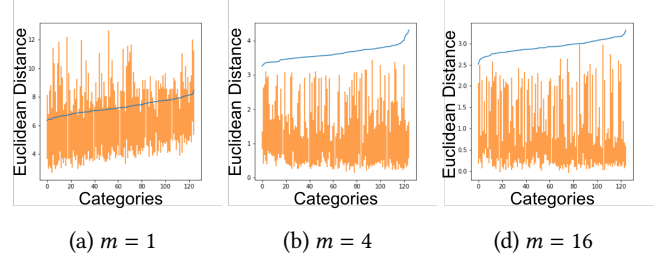


Figure 9: Visualization of inter-class and intra-class distance on Sketchy Extension. The blue lines denote average minimum inter-class distance. The orange bars represent the distribution of intra-class distance of each category.

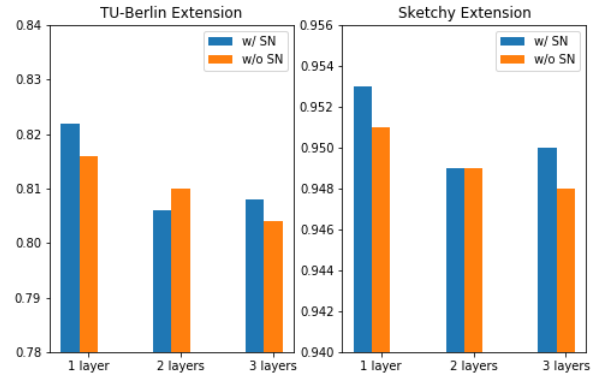


Figure 10: Comparison of MAP results with different settings of \mathcal{F}_{SN} .

shown in Figure 10. We can find that multi-layer networks have worse performance than one-layer linear mapping. Moreover, the spectral normalized networks work better generally, which shows their advantage in maintaining discrimination property.

5 CONCLUSION

In this paper, we have introduced two innovations, including novel network architecture and a loss function. The Domain-Aware Squeeze-and-Excitation (DASE) network allows us to incorporate the domain information of each sample explicitly, while the proposed Multiplicative Euclidean Margin Softmax (MEMS) Loss enables us to learn highly discriminative features which facilitate highly accurate SBIR. Both the architecture and loss are intuitive and simple to implement. On two popular benchmark SBIR datasets, the proposed model has achieved new state-of-the-art results.

ACKNOWLEDGMENTS

This work was supported by the Natural Science Foundation of Guangdong Province(No.2020A1515010711) and the Special Foundation for the Development of Strategic Emerging Industries of Shenzhen(Nos. JCYJ20200109143010272 and JCYJ20200109143035495). This work was supported in part by Science and Technology Commission of Shanghai Municipality Projects (19511120700, 2021SHZDZX0103).

REFERENCES

- [1] Michael M Bronstein, Alexander M Bronstein, Fabrice Michel, and Nikos Paragios. 2010. Data fusion through cross-modality metric learning using similarity-sensitive hashing. In *Computer Vision and Pattern Recognition (CVPR), 2010 IEEE Conference on*. IEEE, 3594–3601.
- [2] Yue Cao, Jiarui Xu, Stephen Lin, Fangyun Wei, and Han Hu. 2019. Gcnnet: Non-local networks meet squeeze-excitation networks and beyond. In *Proceedings of the IEEE International Conference on Computer Vision Workshops*. 0–0.
- [3] Sumit Chopra, Raia Hadsell, and Yann LeCun. 2005. Learning a similarity metric discriminatively, with application to face verification. In *CVPR*.
- [4] Jifeng Dai, Haozhi Qi, Yuwen Xiong, Yi Li, Guodong Zhang, Han Hu, and Yichen Wei. 2017. Deformable convolutional networks. In *Proceedings of the IEEE international conference on computer vision*. 764–773.
- [5] Navneet Dalal and Bill Triggs. 2005. Histograms of oriented gradients for human detection. In *Computer Vision and Pattern Recognition, 2005. CVPR 2005. IEEE Computer Society Conference on*, Vol. 1. IEEE, 886–893.
- [6] Jiankang Deng, Jia Guo, Niannan Xue, and Stefanos Zafeiriou. 2019. Arcface: Additive angular margin loss for deep face recognition. In *Proceedings of the IEEE Conference on Computer Vision and Pattern Recognition*. 4690–4699.
- [7] Guiguang Ding, Yuchen Guo, and Jile Zhou. 2014. Collective matrix factorization hashing for multimodal data. In *Proceedings of the IEEE conference on computer vision and pattern recognition*. 2075–2082.
- [8] Mathias Eitz, James Hays, and Marc Alexa. 2012. How do humans sketch objects? *ACM Trans. Graph.* 31, 4 (2012), 44–1.
- [9] Raia Hadsell, Sumit Chopra, and Yann LeCun. 2006. Dimensionality reduction by learning an invariant mapping. In *null*. IEEE, 1735–1742.
- [10] Junlin Hu, Jiwen Lu, and Yap-Peng Tan. 2014. Discriminative deep metric learning for face verification in the wild. In *Proceedings of the IEEE conference on computer vision and pattern recognition*. 1875–1882.
- [11] Jie Hu, Li Shen, and Gang Sun. 2017. Squeeze-and-excitation networks. *arXiv preprint arXiv:1709.01507* 7 (2017).
- [12] Rui Hu, Mark Barnard, and John Collomosse. 2010. Gradient field descriptor for sketch based retrieval and localization. In *Image Processing (ICIP), 2010 17th IEEE International Conference on*. IEEE, 1025–1028.
- [13] Max Jaderberg, Karen Simonyan, Andrew Zisserman, et al. 2015. Spatial transformer networks. In *Advances in Neural Information Processing Systems*. 2017–2025.
- [14] Qing-Yuan Jiang and Wu-Jun Li. 2016. Deep cross-modal hashing. *CoRR* (2016).
- [15] Toshikazu Kato, Takio Kurita, Nobuyuki Otsu, and Kyoji Hirata. 1992. A sketch retrieval method for full color image database-query by visual example. In *Pattern Recognition, 1992. Vol. 1. Conference A: Computer Vision and Applications, Proceedings., 11th IAPR International Conference on*. IEEE, 530–533.
- [16] Diederik P Kingma and Jimmy Ba. 2014. Adam: A method for stochastic optimization. *arXiv preprint arXiv:1412.6980* (2014).
- [17] Shaishav Kumar and Raghavendra Udupa. 2011. Learning hash functions for cross-view similarity search. In *IJCAI proceedings-international joint conference on artificial intelligence*, Vol. 22. 1360.
- [18] Jiangtong Li, Zhixin Ling, Li Niu, and Liqing Zhang. 2019. Bi-directional domain translation for zero-shot sketch-based image retrieval. *arXiv preprint arXiv:1911.13251* (2019).
- [19] Xiang Li, Wenhui Wang, Xiaolin Hu, and Jian Yang. 2019. Selective kernel networks. In *Proceedings of the IEEE conference on computer vision and pattern recognition*. 510–519.
- [20] Shengcai Liao, Yang Hu, Xiangyu Zhu, and Stan Z Li. 2015. Person re-identification by local maximal occurrence representation and metric learning. In *Proceedings of the IEEE conference on computer vision and pattern recognition*. 2197–2206.
- [21] Hangyu Lin, Yanwei Fu, Peng Lu, Shaogang Gong, Xiangyang Xue, and Yu-Gang Jiang. 2019. Tc-net for isbir: Triplet classification network for instance-level sketch based image retrieval. In *Proceedings of the 27th ACM International Conference on Multimedia*. 1676–1684.
- [22] Zijia Lin, Guiguang Ding, Mingqing Hu, and Jianmin Wang. 2015. Semantics-preserving hashing for cross-view retrieval. In *Proceedings of the IEEE conference on computer vision and pattern recognition*. 3864–3872.
- [23] Huawen Liu, Zongjie Ma, Jianmin Han, Zhongyu Chen, and Zhonglong Zheng. 2018. Regularized partial least squares for multi-label learning. *International Journal of Machine Learning and Cybernetics* 9, 2 (2018), 335–346.
- [24] Li Liu, Fumin Shen, Yuming Shen, Xianglong Liu, and Ling Shao. 2017. Deep sketch hashing: Fast free-hand sketch-based image retrieval. In *Proc. CVPR*. 2862–2871.
- [25] Weiyang Liu, Yandong Wen, Zhiding Yu, Ming Li, Bhiksha Raj, and Le Song. 2017. Sphreface: Deep hypersphere embedding for face recognition. In *The IEEE Conference on Computer Vision and Pattern Recognition (CVPR)*, Vol. 1. 1.
- [26] Weiyang Liu, Yandong Wen, Zhiding Yu, and Meng Yang. 2016. Large-Margin Softmax Loss for Convolutional Neural Networks.. In *icml*. 507–516.
- [27] David G Lowe. 1999. Object recognition from local scale-invariant features. In *Computer vision, 1999. The proceedings of the seventh IEEE international conference on*, Vol. 2. Ieee, 1150–1157.
- [28] Jiwen Lu, Gang Wang, Weihong Deng, Pierre Moulin, and Jie Zhou. 2015. Multi-manifold deep metric learning for image set classification. In *Proceedings of the IEEE conference on computer vision and pattern recognition*. 1137–1145.
- [29] Anubha Pandey, Ashish Mishra, Vinay Kumar Verma, Anurag Mittal, and Hema Murthy. 2020. Stacked Adversarial Network for Zero-Shot Sketch based Image Retrieval. In *The IEEE Winter Conference on Applications of Computer Vision*. 2540–2549.
- [30] Yonggang Qi, Yi-Zhe Song, Honggang Zhang, and Jun Liu. 2016. Sketch-based image retrieval via siamese convolutional neural network. In *Image Processing (ICIP), 2016 IEEE International Conference on*. IEEE, 2460–2464.
- [31] Jose M Saavedra. 2014. Sketch based image retrieval using a soft computation of the histogram of edge local orientations (S-HELO). In *Image Processing (ICIP), 2014 IEEE International Conference on*. IEEE, 2998–3002.
- [32] Jose M Saavedra, Juan Manuel Barrios, and S Orand. 2015. Sketch based Image Retrieval using Learned KeyShapes (LKS).. In *BMVC*, Vol. 1. 7.
- [33] Patson Sangkloy, Nathan Burnell, Cusuh Ham, and James Hays. 2016. The sketchy database: learning to retrieve badly drawn bunnies. *ACM Transactions on Graphics (TOG)* 35, 4 (2016), 119.
- [34] Florian Schroff, Dmitry Kalenichenko, and James Philbin. 2015. Facenet: A unified embedding for face recognition and clustering. In *Proceedings of the IEEE conference on computer vision and pattern recognition*. 815–823.
- [35] Yuming Shen, Li Liu, Fumin Shen, and Ling Shao. 2018. Zero-Shot Sketch-Image Hashing. In *Proceedings of the IEEE Conference on Computer Vision and Pattern Recognition*. 3598–3607.
- [36] Jake Snell, Kevin Swersky, and Richard Zemel. 2017. Prototypical networks for few-shot learning. In *Advances in Neural Information Processing Systems*. 4077–4087.
- [37] Jifei Song, Yu Qian, Yi-Zhe Song, Tao Xiang, and Timothy Hospedales. 2017. Deep spatial-semantic attention for fine-grained sketch-based image retrieval. In *ICCV*.
- [38] Rahul Rama Vario, Mrinal Haloi, and Gang Wang. 2016. Gated Siamese Convolutional Neural Network Architecture for Human Re-Identification. In *ECCV*.
- [39] Javier Via, Ignacio Santamaria, and Jesús Pérez. 2005. Canonical correlation analysis (CCA) algorithms for multiple data sets: Application to blind SIMO equalization. In *Signal Processing Conference, 2005 13th European*. IEEE, 1–4.
- [40] Fang Wang, Le Kang, and Yi Li. 2015. Sketch-based 3d shape retrieval using convolutional neural networks. In *Proceedings of the IEEE Conference on Computer Vision and Pattern Recognition*. 1875–1883.
- [41] Hao Wang, Yitong Wang, Zheng Zhou, Xing Ji, Zhifeng Li, Dihong Gong, Jingchao Zhou, and Wei Liu. 2018. CosFace: Large margin cosine loss for deep face recognition. *arXiv preprint arXiv:1801.09414* (2018).
- [42] Jiang Wang, Yang Song, Thomas Leung, Chuck Rosenberg, Jingbin Wang, James Philbin, Bo Chen, and Ying Wu. 2014. Learning fine-grained image similarity with deep ranking. In *Proceedings of the IEEE Conference on Computer Vision and Pattern Recognition*. 1386–1393.
- [43] Liwei Wang, Yin Li, and Svetlana Lazebnik. 2016. Learning Deep Structure-Preserving Image-Text Embeddings. In *CVPR*.
- [44] Xiaolong Wang, Ross Girshick, Abhinav Gupta, and Kaiming He. 2018. Non-local neural networks. In *Proceedings of the IEEE conference on computer vision and pattern recognition*. 7794–7803.
- [45] Yandong Wen, Kaipeng Zhang, Zhifeng Li, and Yu Qiao. 2016. A discriminative feature learning approach for deep face recognition. In *European Conference on Computer Vision*. Springer, 499–515.
- [46] Wenxuan Xie, Yuxin Peng, and Jianguo Xiao. 2014. Cross-View Feature Learning for Scalable Social Image Analysis.. In *AAAI*. 201–207.
- [47] Sasi Kiran Yelamarthi, Shiva Krishna Reddy, Ashish Mishra, and Anurag Mittal. 2018. A Zero-Shot Framework for Sketch Based Image Retrieval.. In *European Conference on Computer Vision*. Springer, Cham, 316–333.
- [48] Qian Yu, Feng Liu, Yi-Zhe Song, Tao Xiang, Timothy M Hospedales, and Chen-Change Loy. 2016. Sketch me that shoe. In *Proceedings of the IEEE Conference on Computer Vision and Pattern Recognition*. 799–807.
- [49] Qian Yu, Yongxin Yang, Feng Liu, Yi-Zhe Song, Tao Xiang, and Timothy M Hospedales. 2017. Sketch-a-net: A deep neural network that beats humans. *International journal of computer vision* 122, 3 (2017), 411–425.
- [50] Qian Yu, Yongxin Yang, Feng Liu, Yi-Zhe Song, Tao Xiang, and Timothy M. Hospedales. 2017. Sketch-a-Net: a Deep Neural Network that Beats Humans. *IJCV* (2017).
- [51] Dongqing Zhang and Wu-Jun Li. 2014. Large-Scale Supervised Multimodal Hashing with Semantic Correlation Maximization.. In *AAAI*, Vol. 1. 7.
- [52] Hua Zhang, Si Liu, Changqing Zhang, Wenqi Ren, Rui Wang, and Xiaochun Cao. 2016. Sketchnet: Sketch classification with web images. In *Proceedings of the IEEE Conference on Computer Vision and Pattern Recognition*. 1105–1113.
- [53] Jingyi Zhang, Fumin Shen, Li Liu, Fan Zhu, Mengyang Yu, Ling Shao, Heng Tao Shen, and Luc Van Gool. 2018. Generative Domain-Migration Hashing for Sketch-to-Image Retrieval. In *Proceedings of the European Conference on Computer Vision (ECCV)*. 297–314.

6 APPENDIX: THEORETICAL ANALYSIS OF MEMS LOSS

In this section, we will (1) give a formal definition of maximum intra-class distance and minimum inter-class distance; (2) show that for margin m in MEMS loss, $m \geq 2 + \sqrt{3}$ is sufficient and necessary to ensure that the maximum intra-class distance is smaller than minimum inter-class distance, regardless of the number of categories.

6.1 Definition

Since we treat both sketch and photo as instances, we define the merged dataset as:

$$\mathcal{D} = \{(x_i, y_{x_i}) \mid y_{x_i} \in \mathcal{Y}\}_{i=1}^{n_1+n_2} \quad \text{where} \quad \begin{cases} x_i = \mathcal{F}_p(p_i), y_{x_i} = y_{p_i} & \text{if } i \leq n_1 \\ x_i = \mathcal{F}_s(s_{i-n_1}), y_{x_i} = y_{s_{i-n_1}} & \text{if } i > n_1 \end{cases} \quad (8)$$

where \mathcal{F}_p and \mathcal{F}_s are mappings that map photos/sketches into a feature space; n_1, n_2 represent the number of photos and sketches; p, s and y represent photo, sketch and category respectively. They are detailedly illustrated in Sec. 3. For convenience, we also define $\mathcal{D}_y = \{x \mid (x, y_x) \in \mathcal{D} \wedge y_x = y\}$.

Maximum Intra-class Distance and Minimum Inter-class Distance. For category $y \in \mathcal{Y}$, the maximum intra-class distance can be defined by

$$\max_{x, x' \in \mathcal{D}_y} d(x, x')$$

and the minimum inter-class distance:

$$\min_{x \in \mathcal{D}_y, x' \in (\bigcup_{y' \neq y} \mathcal{D}_{y'})} d(x, x')$$

Here we give a formulation of our objective, which is the maximum intra-class distance being smaller than minimum inter-class distance, by proposition P_1 :

$$\forall y \in \mathcal{Y}, \quad \max_{x, x' \in \mathcal{D}_y} d(x, x') \leq \min_{x \in \mathcal{D}_y, x' \in (\bigcup_{y' \neq y} \mathcal{D}_{y'})} d(x, x') \quad (9)$$

Solve Problem with MEMS. Instead of optimizing the distance among instances directly as indicated by eq. 9, the proposed MEMS loss uses prototypes $\{c_y\}_{y \in \mathcal{Y}} \subset \mathcal{X}$ to characterize the distribution of instances in feature space. If this MEMS loss is well optimized, instances will be closer to their corresponding prototype than other prototypes in feature space. This relationship can be described as

$$\forall (x, y_x) \in \mathcal{D}, \forall y \in \mathcal{Y} \wedge y \neq y_x, \quad m \cdot d(x, c_y) \leq d(x, c_{y_x}) \quad (10)$$

For convenience, we denote $\mathcal{R}_{y, y'}$ as a region where

$$x \in \mathcal{R}_{y, y'} \Leftrightarrow m \cdot d(x, c_y) \leq d(x, c_{y'})$$

Also, we denote \mathcal{R}_y as a region where

$$x \in \mathcal{R}_y \Leftrightarrow \forall y' \in \mathcal{Y} \wedge y' \neq y, m \cdot d(x, c_y) \leq d(x, c_{y'})$$

It is easy to prove that $\mathcal{R}_y = \bigcap_{y' \neq y} \mathcal{R}_{y, y'}$. Note that if eq. 10 holds,

$$\forall (x, y_x) \in \mathcal{D}, \quad x \in \mathcal{R}_{y_x}$$

and thus we can derive a sufficient condition for P_1 (eq. 9):

$$\forall y \in \mathcal{Y}, \quad \max_{x, x' \in \mathcal{R}_y} d(x, x') \leq \min_{x \in \mathcal{R}_y, x' \in (\bigcup_{y' \neq y} \mathcal{R}_{y'})} d(x, x') \quad (11)$$

We denote eq. 11 as proposition P_2 .

6.2 Finding Boundaries for m

The later induction is based on the assumption that our MEMS loss can be well optimized, *i.e.* eq. 10 holds, and the assumption that $m \geq 1$. Now the question is: what is the range of m that is sufficient and necessary for P_2 ? In the rest of this section, we firstly calculate the closed form of $\mathcal{R}_{y, y'}$ and then prove that if $m = m_0 \Rightarrow P_2$, then $m = m_0 + \varepsilon \Rightarrow P_2, \forall \varepsilon > 0$. To this end, we only need to find the lower bound of m , with regard to the number of categories: $m_{\min}^{(|\mathcal{Y}|)}$. Next, we prove $m_{\min}^{(2)} = 2 + \sqrt{3}$. Finally, we prove $m_{\min}^{(k)} = 2 + \sqrt{3}, \forall k \geq 3$ is sufficient and necessary for P_2 .

Lemma 1. If $d(x, x') = \|x - x'\|_2$, $\mathcal{R}_{y, y'}$ is a n-ball (ball in n-dimensional space) with center $(c_y + \frac{c_y - c_{y'}}{m^2 - 1})$ and radius $(\frac{m}{m^2 - 1}) \|c_y - c_{y'}\|_2$

Proof If $\mathbf{x} \in \mathcal{R}_{y,y'}$,

$$\begin{aligned}
& m \|\mathbf{x} - \mathbf{c}_y\|_2 \leq \|\mathbf{x} - \mathbf{c}_{y'}\|_2 \\
\Leftrightarrow & m^2 \|\mathbf{x} - \mathbf{c}_y\|_2 \leq \|\mathbf{x} - \mathbf{c}_{y'}\|_2 \\
\Leftrightarrow & m^2 (\mathbf{x}^T \mathbf{x} - 2\mathbf{c}_y^T \mathbf{x} + \mathbf{c}_y^T \mathbf{c}_y) \leq \mathbf{x}^T \mathbf{x} - 2\mathbf{c}_{y'}^T \mathbf{x} + \mathbf{c}_{y'}^T \mathbf{c}_{y'} \\
\Leftrightarrow & (m^2 - 1) \mathbf{x}^T \mathbf{x} - 2(m^2 \mathbf{c}_y^T - \mathbf{c}_{y'}^T) \mathbf{x} \leq \mathbf{c}_{y'}^T \mathbf{c}_{y'} - m^2 \mathbf{c}_y^T \mathbf{c}_y \\
\Leftrightarrow & \left\| \mathbf{x} - \frac{m^2 \mathbf{c}_y - \mathbf{c}_{y'}}{m^2 - 1} \right\|_2^2 \leq \frac{(m^2 - 1)(\mathbf{c}_{y'}^T \mathbf{c}_{y'} - m^2 \mathbf{c}_y^T \mathbf{c}_y) + \|m^2 \mathbf{c}_y - \mathbf{c}_{y'}\|_2^2}{(m^2 - 1)^2} \\
\Leftrightarrow & \left\| \mathbf{x} - \frac{(m^2 - 1)\mathbf{c}_y + \mathbf{c}_{y'} - \mathbf{c}_{y'}}{m^2 - 1} \right\|_2^2 \leq \left(\frac{m}{m^2 - 1} \right)^2 \|\mathbf{c}_y - \mathbf{c}_{y'}\|_2^2 \\
\Leftrightarrow & \left\| \mathbf{x} - \left(\mathbf{c}_y + \frac{\mathbf{c}_{y'} - \mathbf{c}_y}{m^2 - 1} \right) \right\|_2 \leq \left(\frac{m}{m^2 - 1} \right) \|\mathbf{c}_y - \mathbf{c}_{y'}\|_2
\end{aligned}$$

Lemma 2. If $m = m_0 \Rightarrow P_2$, then $m = m_0 + \varepsilon \Rightarrow P_2, \forall \varepsilon > 0$

Proof With $m = m_0$ slightly expanding to $m = m_0 + \varepsilon$, region $\mathcal{R}_{y,y'}$ becomes $\mathcal{R}'_{y,y'}$, where

$$\forall \mathbf{x} \in \mathcal{R}'_{y,y'}, \quad d(\mathbf{x}, \mathbf{c}_{y'}) \geq (m_0 + \varepsilon) d(\mathbf{x}, \mathbf{c}_y) \geq m_0 d(\mathbf{x}, \mathbf{c}_y)$$

So we can conclude that $\mathcal{R}'_{y,y'} \subseteq \mathcal{R}_{y,y'}$. Thus

$$\forall y \in \mathcal{Y}, \quad \mathcal{R}'_y = \bigcap_{y' \neq y} \mathcal{R}'_{y,y'} \subseteq \bigcap_{y' \neq y} \mathcal{R}_{y,y'} = \mathcal{R}_y \quad (12)$$

Now we rewrite P_2 as

$$\forall y \in \mathcal{Y}, \forall y' \in \mathcal{Y} \wedge y' \neq y, \quad \max_{\mathbf{x}, \mathbf{x}' \in \mathcal{R}_y} d(\mathbf{x}, \mathbf{x}') \leq \min_{\mathbf{x} \in \mathcal{R}_y, \mathbf{x}' \in \mathcal{R}_{y'}} d(\mathbf{x}, \mathbf{x}') \quad (13)$$

Since eq. 12,

$$\begin{aligned}
\max_{\mathbf{x}, \mathbf{x}' \in \mathcal{R}'_y} d(\mathbf{x}, \mathbf{x}') & \leq \max_{\mathbf{x}, \mathbf{x}' \in \mathcal{R}_y} d(\mathbf{x}, \mathbf{x}') \\
\min_{\mathbf{x} \in \mathcal{R}'_y, \mathbf{x}' \in \mathcal{R}'_{y'}} d(\mathbf{x}, \mathbf{x}') & \geq \min_{\mathbf{x} \in \mathcal{R}_y, \mathbf{x}' \in \mathcal{R}_{y'}} d(\mathbf{x}, \mathbf{x}')
\end{aligned}$$

which means if eq. 13 holds for $m = m_0$, it also holds for $m = m_0 + \varepsilon$.

Lemma 3. $m_{\min}^{(2)} = 2 + \sqrt{3}$ is sufficient and necessary for P_2 .

Proof We can write $\mathcal{Y} = \{1, 2\}$. Now $\mathcal{R}_1 = \mathcal{R}_{1,2}, \mathcal{R}_2 = \mathcal{R}_{2,1}$, which are two n-balls with same radius and different centers. The maximum intra-class distance is the diameter of each n-ball:

$$\forall y \in \mathcal{Y}, \quad \max_{\mathbf{x}, \mathbf{x}' \in \mathcal{R}_y} d(\mathbf{x}, \mathbf{x}') = \left(\frac{2m}{m^2 - 1} \right) \|\mathbf{c}_1 - \mathbf{c}_2\|_2$$

The minimum inter-class distance is the distance between two centers minus the diameter:

$$\begin{aligned}
\forall y \in \mathcal{Y}, \quad \min_{\mathbf{x} \in \mathcal{R}_y, \mathbf{x}' \in \left(\bigcup_{y' \neq y} \mathcal{R}_{y'} \right)} d(\mathbf{x}, \mathbf{x}') & = \left\| \left(\mathbf{c}_1 + \frac{\mathbf{c}_1 - \mathbf{c}_2}{m^2 - 1} \right) - \left(\mathbf{c}_2 + \frac{\mathbf{c}_2 - \mathbf{c}_1}{m^2 - 1} \right) \right\|_2 - \left(\frac{2m}{m^2 - 1} \right) \|\mathbf{c}_1 - \mathbf{c}_2\|_2 \\
& = \left(\frac{m^2 - 2m + 1}{m^2 - 1} \right) \|\mathbf{c}_1 - \mathbf{c}_2\|_2
\end{aligned}$$

Let $\left(\frac{m^2 - 2m + 1}{m^2 - 1} \right) \|\mathbf{c}_1 - \mathbf{c}_2\|_2 \geq \left(\frac{2m}{m^2 - 1} \right) \|\mathbf{c}_1 - \mathbf{c}_2\|_2$, we can get the result $m \geq 2 + \sqrt{3}$ or $m \leq 2 - \sqrt{3}$. We abandon the latter solution since only when $m \geq 1$ does it make sense. So in binary class case, $m \geq m_{\min}^{(2)} = 2 + \sqrt{3}$ if sufficient and necessary for P_2 .

Lemma 4. $m_{\min}^{(k)} = 2 + \sqrt{3}, \forall k \geq 3$ is necessary for P_2 .

Proof Consider an extreme condition, where two prototypes $\mathbf{c}_{y_a}, \mathbf{c}_{y_b}$ are far from the other prototypes. We notice that

$$\forall y \in \mathcal{Y} \wedge y \neq y_a \wedge y \neq y_b, \|\mathbf{c}_{y_a} - \mathbf{c}_y\|_2 \geq \frac{m+1}{m-1} \|\mathbf{c}_{y_a} - \mathbf{c}_{y_b}\|_2 \Rightarrow \min_{\mathbf{x} \in \mathcal{R}_{y_a, y}} d(\mathbf{x}, \mathbf{c}_{y_a}) \geq \max_{\mathbf{x} \in \mathcal{R}_{y_a, y_b}} d(\mathbf{x}, \mathbf{c}_{y_a}) \Rightarrow \mathcal{R}_{y_a, y_b} \subseteq \mathcal{R}_{y_a, y}$$

Since we have no constraints on location of prototypes, this condition can always be likely to hold, regardless of the value of m . When all the rest prototypes satisfy this condition for both $\mathbf{c}_{y_a}, \mathbf{c}_{y_b}$, we have $\mathcal{R}_{y_a} = \mathcal{R}_{y_a, y_b}$ and $\mathcal{R}_{y_b} = \mathcal{R}_{y_b, y_a}$, which is same as in binary case. So $m \geq m_{\min}^{(2)}$ becomes necessary to ensure the correctness of P_2 , and thus Lemma 4 is true.

Lemma 5. $m_{\min}^{(k)} = 2 + \sqrt{3}, \forall k \geq 3$ is sufficient for P_2 .

Proof If we want to prove that P_2 (eq. 13) holds, we have to show that every distinct pair (y_a, y_b) satisfy $\max_{\mathbf{x}, \mathbf{x}' \in \mathcal{R}_{y_a}} d(\mathbf{x}, \mathbf{x}') \leq \min_{\mathbf{x} \in \mathcal{R}_{y_a}, \mathbf{x}' \in \mathcal{R}_{y_b}} d(\mathbf{x}, \mathbf{x}')$. We remove a category y_c , where $y_c \neq y_a$ and $y_c \neq y_b$, from \mathcal{Y} and forms \mathcal{Y}' such that $|\mathcal{Y}'| = |\mathcal{Y}| - 1$. Suppose $m = m_{\min}^{(|\mathcal{Y}'|)}$ satisfies eq. 13, we have

$$\begin{aligned} \max_{\mathbf{x}, \mathbf{x}' \in \mathcal{R}'_{y_a}} d(\mathbf{x}, \mathbf{x}') &\leq \min_{\mathbf{x} \in \mathcal{R}'_{y_a}, \mathbf{x}' \in \mathcal{R}'_{y_b}} d(\mathbf{x}, \mathbf{x}') \\ \text{where } \mathcal{R}'_{y_a} &= \bigcap_{y \in \mathcal{Y}', y \neq y_a} \mathcal{R}_{y_a, y} = \bigcap_{y \in \mathcal{Y}, y \neq y_a, y \neq y_c} \mathcal{R}_{y_a, y} \quad , \\ \mathcal{R}'_{y_b} &= \bigcap_{y \in \mathcal{Y}', y \neq y_b} \mathcal{R}_{y_b, y} = \bigcap_{y \in \mathcal{Y}, y \neq y_b, y \neq y_c} \mathcal{R}_{y_b, y} \end{aligned}$$

When m is not changed and prototypes are not moved,

$$\begin{aligned} \mathcal{R}_{y_a} &= \bigcap_{y \in \mathcal{Y}, y \neq y_a} \mathcal{R}_{y_a, y} \subseteq \bigcap_{y \in \mathcal{Y}, y \neq y_a, y \neq y_c} \mathcal{R}_{y_a, y} = \mathcal{R}'_{y_a} \\ \mathcal{R}_{y_b} &= \bigcap_{y \in \mathcal{Y}, y \neq y_b} \mathcal{R}_{y_b, y} \subseteq \bigcap_{y \in \mathcal{Y}, y \neq y_b, y \neq y_c} \mathcal{R}_{y_b, y} = \mathcal{R}'_{y_b} \end{aligned}$$

and

$$\begin{aligned} \mathcal{R}_{y_a} \subseteq \mathcal{R}'_{y_a} &\Rightarrow \max_{\mathbf{x}, \mathbf{x}' \in \mathcal{R}_{y_a}} d(\mathbf{x}, \mathbf{x}') \leq \max_{\mathbf{x}, \mathbf{x}' \in \mathcal{R}'_{y_a}} d(\mathbf{x}, \mathbf{x}') \\ \mathcal{R}_{y_a} \subseteq \mathcal{R}'_{y_a} \wedge \mathcal{R}_{y_b} \subseteq \mathcal{R}'_{y_b} &\Rightarrow \min_{\mathbf{x} \in \mathcal{R}_{y_a}, \mathbf{x}' \in \mathcal{R}_{y_b}} d(\mathbf{x}, \mathbf{x}') \geq \min_{\mathbf{x} \in \mathcal{R}'_{y_a}, \mathbf{x}' \in \mathcal{R}'_{y_b}} d(\mathbf{x}, \mathbf{x}') \end{aligned}$$

Thus, $\max_{\mathbf{x}, \mathbf{x}' \in \mathcal{R}_{y_a}} d(\mathbf{x}, \mathbf{x}') \leq \min_{\mathbf{x} \in \mathcal{R}_{y_a}, \mathbf{x}' \in \mathcal{R}_{y_b}} d(\mathbf{x}, \mathbf{x}')$ is satisfied for any pair (y_a, y_b) where $y_a, y_b \in \mathcal{Y}$, even if we directly adopt $m = m_{\min}^{(|\mathcal{Y}'|)}$ when $|\mathcal{Y}| = |\mathcal{Y}'| + 1$. So we can conclude that $m_{\min}^{(|\mathcal{Y}'|)} \geq m_{\min}^{(|\mathcal{Y}'|+1)}$ is sufficient for P_2 . By Lemma 3, $m_{\min}^{(2)} = 2 + \sqrt{3}$, we can conclude that $m_{\min}^{(k)} = 2 + \sqrt{3}, \forall k \geq 3$ is sufficient for P_2 .